Aqueous Zirconium-MOF Synthesis Assisted by α-Cyclodextrin: Towards Deeper Understanding of the Beneficial Role of Cyclodextrin

Guillaume Hoyez, Cyril Rousseau, Jolanta Rousseau, Sébastien Saitzek, Anne Ponchel, Eric Monflier

Aqueous zirconium-MOF syntheses assisted by α-cyclodextrin: towards deeper understanding of the beneficial role of cyclodextrin

Guillaume Hoyez,[a] Cyril Rousseau,[a] Jolanta Rousseau,[a] Sébastien Saitzek,[a] Anne Ponchel,[a] and Eric Monflier*[a]

Dedication ((optional))

[a] G. Hoyez, Dr. C. Rousseau, Dr. J. Rousseau, Prof. Dr. S. Saitzek, Prof. Dr. A. Ponchel and Prof. Dr. E. Monflier*
Univ. Artois, CNRS, Centrale Lille, Univ. Lille, UMR 8181 – UCCS – Unité de Catalyse et Chimie du Solide
Faculté des Sciences Jean Perrin, Rue Jean Souvraz SP 18
F-62300 Lens, France
E-mail: eric.monflier@univ-artois

Supporting information for this article is given via a link at the end of the document.

Abstract: A series of isoreticular zirconium-organic frameworks based on the UiO-66 family have been synthesised through a co-modulated hydrothermal method. Our synthetic approach relies on the use of α-cyclodextrin to co-modulate the morphology and size of the UiO-66 analogues. We have undertaken a systematic study aiming at exploring how the addition of α-CD to the reaction mixture can affect or not the morphology of UiO-66 Zr-MOFs, choosing various substituted benzene-1,4-dicarboxylic acids and pyridine-2,5-dicarboxylic acid as representative organic linkers. The proportion of α-CD with respect to each ligand can be easily tuned during synthesis, and depending on the chemical structure of the ligands, the oligosaccharide is found to substantially impact the characteristics of the UiO-66 derivatives. A rationale is proposed to explain the crucial role that α-CD plays, considering that one of the key parameters is the water solubility of the organic linkers.

Introduction

Metal-Organic Frameworks (MOFs) are a unique type of crystalline coordination polymers of two-dimensional (2D) or three-dimensional (3D) networks, constructed from metal-oxo clusters (also termed metal nodes) bridged together by multidentate organic linkers. Since the early 1990s, MOFs are the subject of increasing attention because of their outstanding chemical and physical features associated to extremely high porosities and surface areas, adjustable pore sizes and functionalizable environments. The structural organization is dependent on the choice of metal source and organic linkers, which gives chemists the possibility of designing an almost infinite variety of MOF architectures. A large number of metals have been explored for the synthesis of MOFs,[1] ranging from alkaline or earth metals (K, Rb, Cs) to poor metals (Al, Ga, In) to transition metals (Zr, Ti, Hf, W, Cu, Fe or Zn) and even lanthanides (Ce, Eu).

In this way, several thousands of MOFs are synthetically accessible through an unlimited combination of metal nodes and organic linkers as well as a large diversity of synthesis methods.[2] In addition to their structural uniformity and permanent ordered porosity, MOFs may also possess several other desirable properties, which render them highly attractive for a wide range of applications, including for example gas storage and/or separation, drug delivery, biomedicine, luminescence, or heterogeneous catalysis,[3] Comprehensive overviews of the various facets of the MOF chemistry can be found in excellent reviews.[4] In terms of preparation, one of the main challenges is to establish synthetic routes under greener and more sustainable conditions. Indeed, most of the described MOFs frequently suffer from harsh synthetic conditions, generally requiring high pressures (batch synthesis) and temperatures (typically above 120°C) and long synthesis durations. Furthermore, the typical solvent is N,N-dimethylformamide (DMF).

Among the large panel of existing MOFs, Zr-MOFs have received a substantially increasing interest in recent years due to their remarkable properties including low toxicity, environmentally friendly nature, and stability (chemical, thermal and hydrothermal stability.[5] The most common are certainly those belonging to the UiO-66 series (UiO for Oslo University). UiO-66 (Zr) was first synthesized by Lillerud et al. in 2008,[6] and its structure consists of octahedral hexanuclear zirconium-oxo clusters ($Zr_6O_4(OH)_4$) connected by twelve 1,4-benzenedicarboxylates as linear bridging ligands. These dicarboxylate groups are directly derived from terephthalic acid to afford a crystalline porous 3D network with a face-centered cubic symmetry (fcu topology). Notably, the possibility of using functionalized 1,4-benzene-dicarboxylate linkers in order to develop a family of isoreticular MOFs based on the standard UiO-66 structure, with tailored properties, has also been demonstrated. This derivatization strategy has proved to be fruitful with a wide range of pendant functional groups, allowing the formation of diverse Zr-based UiO-66 materials, such as for example UiO-66-NH_2, UiO-66-NO_2 or UiO-66-Br.

In the first synthesis protocol reported in the literature,[6] UiO-66 has been synthesized by reacting $ZrCl_4$ with terephthalic acid under autogenous pressure at 120°C for 1 day using DMF as solvent. In such conditions, the major issue comes from the large quantity of corrosive HCl that is generated as a by-product. In the recent literature, alternative approaches towards greener and scalable synthesis, by preventing or minimizing the use of harmful DMF, have appeared. Thus, the impact of the nature of the solvent on the properties of the UiO-66 benchmark has been the subject of a large screening study, with 40 solvents of lower

toxicity and environmental impact as compared to reference DMF. Among the different solvents examined, γ-valerolactone was found to be probably the best for substituting DMF.[7]

In this context, the development of hydrothermal synthesis methods for functionalized UiO-66 materials is also of considerable interest. Reinsch et al.,[8] have successfully developed a hydrothermal synthesis of UiO-66 derivatives, in which DMF was replaced by water in the presence of $Zr(SO_4)_2$ as the metal salt precursor. A recent study has also been focused on the action of pH during MOF crystallization. Thus, Huelsenbeck et al. were able to achieve rapid synthesis of two different MOFs of the UiO series (UiO-66 and UiO-66-NH_2) in water by optimizing the concentrations of metal nodes and deprotonated linker through pH adjustment.[9] Interestingly, other synthetic methods involving the use of microwave irradiations,[10] mechanochemical activations [11] or microflow chemistry [12] have also been proposed for accelerating the formation of some archetypal metal-based organic frameworks, such as UiO-type MOFs, within few minutes. Some of us have also reported that synthesizing UiO-66-NH_2 from the disodium salt of 2-aminoterephthalate in ambient aqueous conditions using acetic acid modulator resulted in a material with a high surface area (888 $m^2 \cdot g^{-1}$),[13] comparable to that obtained under classical hydrothermal syntheses.[14] Recently, our group explored the possibility of using of cyclodextrins (cyclic oligosaccharides constituted of α-D-glucopyranose units) through a modulated hydrothermal approach to influence the porous properties of UiO-66-NH_2. It was observed that, after optimization of the synthesis conditions, the BET surface area of the final Zr-MOF materials could be almost doubled (1451 $m^2 \cdot g^{-1}$) through the addition of 1 equivalent of α-CD with respect to the 2-aminoterephthalic acid linker. This effect was related to the role of this cyclodextrin during the synthesis process, playing a co-modulator role to control the nucleation and growth of the hexanuclear Zr-oxo clusters by competing with the linker, but without interacting with it by forming an inclusion complex.[15] In the field of material science, it has been recently discovered that the association of cyclodextrins with various metal ions or inorganic nanostructures could constitute an attractive strategy for controlling the fabrication of hybrid functional nanostructures, hierarchically organized in molecular or in polymeric materials.[16]

In this contribution and in order to further examine the potential scope of α- cyclodextrin in the preparation of Zr-based MOFs in aqueous phase conditions, we have extended the investigation to eight different UiO-66 analogues, by utilizing a variety of substituted benzene or pyridine dicarboxylic acid linkers bearing NH_2, OH, Br, F, NO_2 or COOH as functional groups. The resulting UiO-66 materials, prepared with or without cyclodextrin, have been fully characterized by powder X-ray diffraction and N_2-adsorption-desorption. The synthetic experiments are focused on the development and optimization of UiO-66 materials with the largest specific surface areas through a careful adjustment of the α-CD proportion. We report that the impact of the latter on the textural characteristics of the resulting MOFs may be positive or negative, depending on the chemical structure of the ligands. The insights obtained from this study provide evidence that the solubility of the linker appears as a fundamental factor influencing the connectivity of the Zr-oxo clusters in the UiO-66 crystallization process.

Results and Discussion

In a previous study, in which we sought to optimize the synthesis of UiO-66-NH_2, we found that the simple addition of a controlled amount of α-CD as a co-modulator into the aqueous medium could dramatically improve the textural properties, especially the specific surface areas, of the solid products. Among the different ratios tested, UiO-66-NH_2 prepared with 1 equivalent of α-CD with respect to H_2BDC-NH_2 gave rise to the highest BET specific surface area achieving 1451 $m^2 \cdot g^{-1}$. Inspired by this finding, we have decided in this work to extend the cyclodextrin-assisted methodology on other UiO-66-type MOFs, including UiO-66-$(OH)_2$, UiO-66-Br, UiO-66-PDC, UiO-66-NO_2, UiO-66-$(COOH)_2$, UiO-66-COOH and UiO-66-F_4. Table 1 lists the chemical structure, name and abbreviation of the different dicarboxylic acid linkers used, as well as the nomenclature of the resulting UiO-66 samples. For comparison purpose, a common and general modulated hydrothermal approach for the synthesis of the different pure-phase products has been defined by selecting a set of design parameters. Briefly, the UiO-66-type MOFs materials (also called UiO-66-R) are obtained through the hydrothermal reaction of $ZrOCl_2$ precursor with the dicarboxylic acid (DCA) linker in an equivolume mixture of acetic acid and water (5 mL/5 mL), in the presence or absence of α-CD as the co-modulator. The amounts of Zr(IV)/DCA (1 mmol/1 mmol), solvent (10 mL) and reaction temperature/time (90°C/24 h) are all kept constant. Ultimately the only variable parameter, which has been studied, is the molar ratio of α-CD to DCA linker, with values typically being in the range 0-1 (except for the UiO-66-NH_2 series for which the ratio has been increased up to 2).

Based on our previous observations on the positive impact of α-CD on textural properties of UiO-66-NH_2, the BET surface area of all the hydrothermally synthesized UiO-66-R MOFs has been first determined from the N_2 adsorption isotherms (Figures S1 to S8). The resulting values with increasing α-CD/linker molar ratios (from 0 to 1) are plotted in Figure 1 while the surface area, porosity and N_2 gas uptake properties of these materials are gathered in Table S1 to S8. It should be noticed the BET surface areas were determined by using the four different consistency criteria as described by Rouquerol et al.[17]

As evidenced by Figure 1, it appears that the influence of α-CD on the BET values differs significantly depending on the type of dicarboxylic acid linker used. Thus, two main different categories can be distinguished. The first one corresponds to UiO-66-type MOFs for which BET surface areas are relatively low (< 450 $m^2 \cdot g^{-1}$) and are hardly affected by the addition of α-CD during the synthesis. This includes the following materials: UiO-66-$(COOH)_2$, UiO-66-(COOH) and UiO-66-F_4. Conversely, the second one concerns other UiO-66 derivatives (UiO-66-NH_2, UiO-66-$(OH)_2$, UiO-66-Br, UiO-66-PDC and UiO-66-NO_2) showing an overall increase in the BET surface area upon the addition of α-CD, as compared to the respective controls. Interestingly, these results tend to confirm the relevance of using this oligosaccharide to modulate the textural features of crystalline MOFs. A control over the specific surface areas developed by these materials may be achieved by adjusting the α-CD/linker molar ratio.

Table 1. Chemical structure, name and abbreviation of the linker compounds and corresponding MOF UiO-66-R materials prepared by hydrothermal synthesis.

Linker structure	Linker name	Linker abbreviation	MOF UiO-66-R
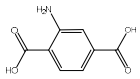	2-aminoterephthalic acid	*H*$_2$BDC-NH$_2$	UiO-66-NH$_2$
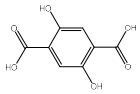	2,5-dihydroxyterephthalic acid	*H*$_2$BDC-(OH)$_2$	UiO-66-(OH)$_2$
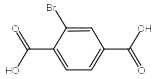	2-bromoterephthalic acid	*H*$_2$BDC-Br	UiO-66-Br
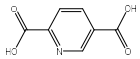	pyridine-2,5-dicarboxylic acid	*H*$_2$PDC	UiO-66-PDC
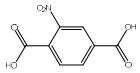	2-nitroterephthalic acid	*H*$_2$BDC-NO$_2$	UiO-66-NO$_2$
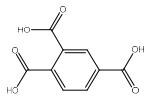	benzene-1,2,4,5-tetracarboxylic acid (Pyromellitic acid)	*H*$_2$BDC-(COOH)$_2$	UiO-66-(COOH)$_2$
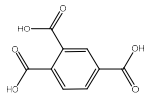	benzene-1,2,4-tricarboxylic acid (Trimellitic acid)	*H*$_2$BDC-COOH	UiO-66-COOH
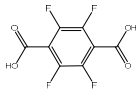	2,3,5,6-tetrafluoroterephthalic acid	*H*$_2$BDC-F$_4$	UiO-66-F$_4$

For instance, for the UiO-66-NH$_2$ and UiO-66-(OH)$_2$, the nitrogen BET surface areas reach their highest values when 1 equivalent of α-CD with respect to each corresponding linker is used (1451 m^2·g^{-1} and 826 m^2·g^{-1} respectively). Regarding the UiO-66-Br and UiO-66-PDC, the samples prepared with the α-CD/linker molar ratio of 0.75 present the best textural characteristics (862 m^2·g^{-1} and 974 m^2·g^{-1} respectively). For the UiO-66-NO$_2$, the uptake of N$_2$ is substantially increased, with a specific surface area reaching 713 m^2·g^{-1} only when a small quantity of α-CD is employed during the synthesis (α-CD/linker molar ratio of 0.25).

To sum up, the BET results indicate that, compared to their parent UiO-66 materials using only acid acetic as the modulator, the gain in specific surface area for the materials prepared with α-CD under optimized conditions is more or less important depending on the chemical structure of the bridging ligand linker, and can be ranked in the following ascending order : UiO-66-Br 0.75 eq α-CD (+ 99 m^2·g^{-1} ~ 13 % increase) < UiO-66-NO$_2$ 0.25 eq α-CD (+ 121 m^2·g^{-1} ~ 20 % increase) < UiO-66-(OH)$_2$ 1 eq α-CD (+ 204 m^2·g^{-1} ~ 30 % increase) < UiO-66-PDC 0.75 eq α-CD (+ 506 m^2·g^{-1} ~108 % increase) < UiO-66-NH$_2$ 1 eq α-CD (+ 840 m^2·g^{-1} ~ 137 % increase).

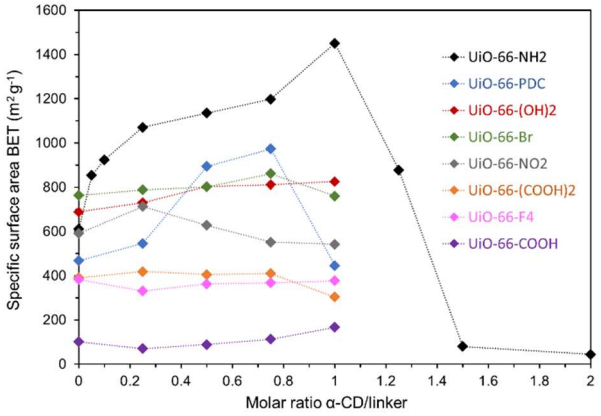

Figure 1. BET specific surface area as a function of the α-CD/linker molar ratio used during the hydrothermal synthesis of the UiO-66-type MOFs. from the bottom to the top, UiO-66-COOH (purple), UiO-66-F$_4$ (pink), UiO-66-(COOH)$_2$ (orange), UiO-66-NO$_2$ (grey), UiO-66-Br (green), UiO-66-(OH)$_2$ (red), UiO-66-PDC and UiO-66-NH$_2$ (black).

In what follows, for the sake of clarity, we will only discuss the results obtained with the five UiO-66-type materials produced at optimized α-CD/linker molar ratios (as above listed). For the three remaining UiO-66-R samples (with R = F$_4$, (COOH)$_2$ and COOH) for which the BET surfaces are little or not affected by the cyclic molecule irrespective of the amount used, the results will be analyzed based on the parent MOFs (i.e. samples prepared without cyclodextrin). It is also worth noting that the full characterization results are available in the supporting information.

To evaluate the porosity of the selected UiO-66 MOF derivatives, textural properties were first examined by N$_2$ adsorption-desorption analyses (Figure 2). All MOF samples display similar type-I isotherms, typical of microporous solids in which most of the pores have a size below 20 Å. Depending on the type of dicarboxylic acid linker used, the resulting porosity and surface area vary between the different families of UiO-66 MOFs. This suggests that the connectivity mechanisms between the hexanuclear Zr-oxo cluster and the DCA linker during MOF crystallization are diverse, probably due in part to the different steric hindrances and different electronic properties (presence of electron-withdrawing and electron-donating groups). For example, *H*$_2$BDC-COOH gives rise to the poorest textural characteristics irrespective of the reaction conditions, exhibiting specific surface areas and total pore volumes as low as 102 m^2·g^{-1} and 0.073 cm^3·g^{-1} (Table S7, ESI). Opposing this behavior, the porosity of Zr-UiO-66-NH$_2$ 1 eq α-CD is significantly higher than that of the other families of Zr-MOFs prepared, with a BET surface area of 1451 m^2·g^{-1}, a total pore volume of 0.575 cm^3·g^{-1} and micropore volume of 0.373 cm^3·g^{-1} (Table S1, ESI).

It should be also emphasized that the specific trend showing the impact of the amount of α-CD on the BET surface area for the UiO-66-NH$_2$ series (Figure 1) can be extended to most the N$_2$ sorption parameters. Indeed, adjusting the addition of α -CD to its optimal ratio of 1 allows the highest Langmuir surface area, micropore volume and micropore surface area and total pore volume. A similar conclusion can be drawn from the results for UiO-66-(OH)$_2$ (Table S2, ESI), UiO-66-Br (Table S3, ESI), UiO-66-PDC (Table S4, ESI) and UiO-66-NO$_2$ (Table S5, ESI). It can, however, be noticed that the proportion of micropores (V_{micro}/V_{total}) within the porous frameworks is not significantly altered by the

utilization of α-CD during the MOF synthesis. Indeed, only the UiO-66-NH_2 1 eq α-CD and UiO-66-NO_2 0.25 eq α-CD samples exhibit a marked increase in the percentage of micropores, from 54.1 % to 64.9 % and, from 47.6 % to 57.2 % respectively, as compared to their analogues synthesized without any α-CD.

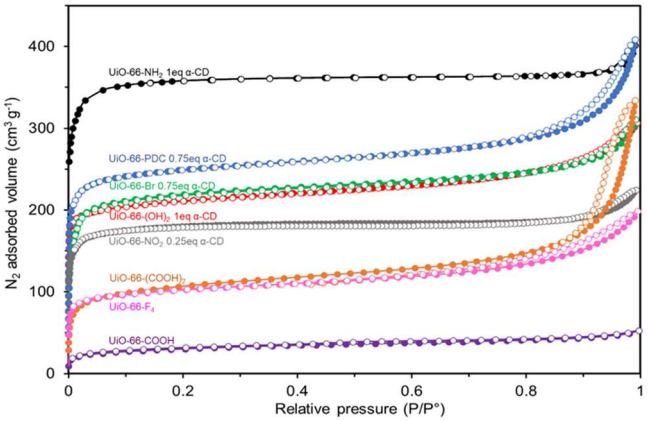

Figure 2. N_2 sorption isotherms collected at 77 K for the selected UiO-66-R materials: from the bottom to the top, UiO-66-COOH (purple), UiO-66-F_4 (pink), UiO-66-$(COOH)_2$ (orange), UiO-66-NO_2 0.25 eq. α-CD (grey), UiO-66-$(OH)_2$ 1 eq. α-CD red), UiO-66-Br 0.75 eq. α-CD (green), UiO-66-PDC 0.75 eq. α-CD (blue) and UiO-66-NH_2 1 eq. α-CD (black). Adsorption (filled circles) and desorption (open circles).

Further evidence of the presence of micropores has been provided from the pore size distributions using the nonlocal density functional theory (NLDFT) and assuming a cylindrical pore geometry (Figure S9, ESI). Thus, the pore size distributions of the UiO-66-R materials (with R = NH_2, PDC, Br, $(OH)_2$ and NO_2) are relatively similar, with pore sizes centred at about 1.1 nm and 1.5 nm. The first category, which is dominant, is assigned to regular octahedral pores whereas the second category can be generated by missing-linker defects, known to enlarge pore sizes. Some slight changes in the small- pore range can also be observed, due to the introduction of additional substituents (F and OH) on the *H*$_2$BDC aromatic ring. In addition, a lower intensity level of micropores (below 2 nm) is revealed on the pore size distributions of UiO-66-$(COOH)_2$, UiO-66-F_4 and UiO-66-(COOH), this trend being consistent with the results of N_2 adsorption capacity and pore volume. Note that a widening of the pore size distribution with the appearance of a very broad contribution centered at about 2.7 nm is also evidenced, suggesting an even higher proportion of missing-linker defects or higher degree of disorder of the porous framework with collapsed pores.

It can be also observed that some of the Zr-MOF samples may undergo a slight deviation from type I-isotherm with capillary condensation at relatively high pressure (P/P° ~0.9) with a H_3-type hysteresis loop, which suggest the existence of larger pores formed between particles of unequal sizes and irregular forms. These hystereses, which appear more prominently with the UiO-66-F_4, UiO-66-$(COOH)_2$ and UiO-66-PDC structures, could be a sign of higher disturbance in the nucleation, growth and agglomeration of the corresponding MOF particles. In the former two cases, this can be indicative of additional steric hindrance generated on the pyromellitic acid and tetrafluoroterephthalic acid, which can lead to the creation of more defects, such as pending linkers, missing-linker defects or cluster-missing defects[18,19] For UiO-66-PDC, the hysteresis may originate from the occurrence of preferential interactions between α-CD and the PDC linker (pyridine-2,5-dicarboxylic acid) in the form of inclusion and external complexes.[20] These interactions may disturb the growth process as a result of secondary or incomplete reactions that ultimately induce more defects within the framework.

Powder X-ray diffraction (XRD) analysis was further performed to examine the crystallinity and purity phase of the eight series of UiO-66-type MOFs (Figure 3).

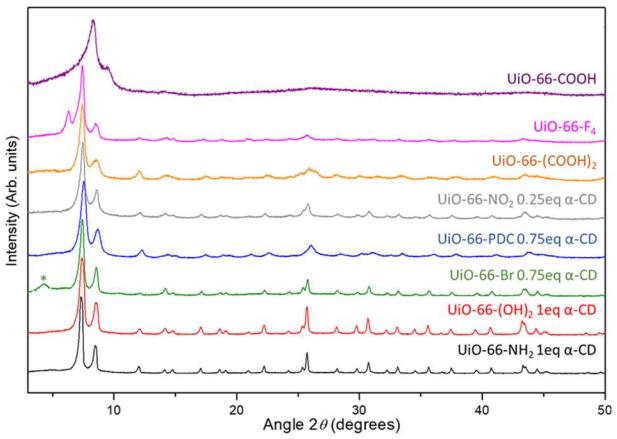

Figure 3. XRD patterns of the selected UiO-66-R materials synthesized using the selected molar ratio of α-CD with respect to the linker. The star symbol is assigned to the reo defect phase.

Except for the solids prepared from *H*$_2$BCD-F_4 and *H*$_2$BCD-COOH that have a poor degree of crystallinity, the XRD patterns of most of the synthesized MOFs are practically identical, exhibiting diffraction lines characteristic of an isostructural UiO-66 framework with a face-centered-cubic fm3m structure.[21] Importantly, within the same series of UiO-66-R solids, no discernible difference emerges from the diffraction patterns as a function of molar the ratio of α-CD to DCA linker (Figures S10 to S17). However, it is noteworthy to mention that the XRD pattern of UiO-66-Br shows the presence of an additional broad peak at 2θ ~ 4°, which is assigned to a formation of short-range ordered reo-phase (marked by a star symbol in Figure 3*).* The appearance of reo nanoregions within the UiO-66 MOF structures is usually related to missing Zr_6 oxo-clusters defects (correlated vacancies) within the UiO-66.[9,22] Initially, the phenomenon of correlations in cluster vacancies in the structure of UiO-66 MOFs was structurally interpreted for UiO-66 (Hf) by means of experimental and computational techniques in the group of Goodwin.[23]

In comparison, a significant loss in the crystallinity and long-range order occur when using *H*$_2$BDC-F4 as the linker, evidenced by the broadening of the diffraction lines. This reflects that, under our synthetic conditions, the additional fluorine atoms in the positions 2,3,5 and 6 of the terephatalic acid scaffold strongly disturb the normal crystallization of the UiO-66 MOF. This is in good agreement with the aforementioned N_2 sorption data.

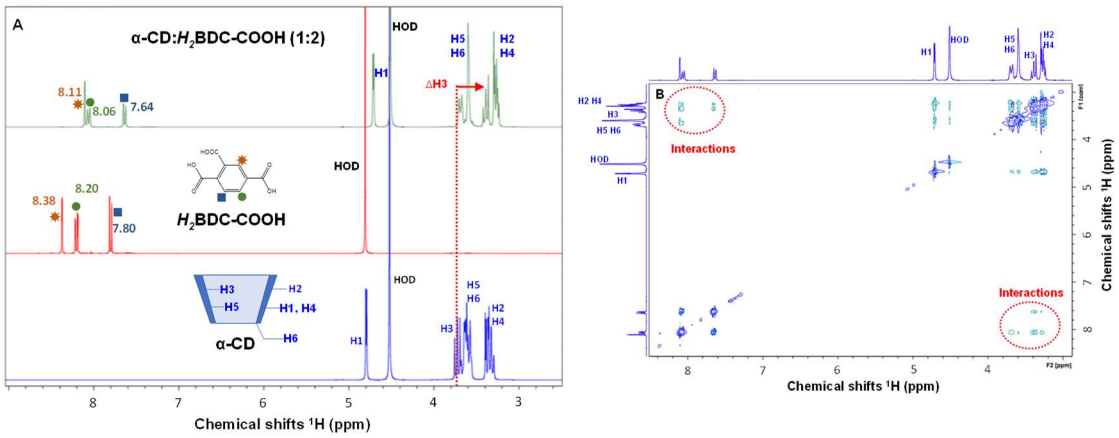

Figure 4. (A) NMR spectra (400 MHz, 25°C, D2O, 1 mM) of α-CD (blue spectrum), *H*$_2$BDC-COOH (red spectrum) and 1/1 mixture of α-CD and *H*$_2$BDC-COOH (green spectrum). (B) Partial contour plot of the T-ROESY spectrum of a D_2O solution containing α-CD and *H*$_2$BDC-COOH at the same concentration (1 mM).

In the literature also, it is found that the use of the tetrafluorinated *H*$_2$BDC linker reduces the degree of crystallinity of the resulting UiO-66 MOF. Actually, a weakening of the chemical bonds between the carboxylates of the organic linker and the Zr_6-oxo clusters has been mentioned, caused by the presence of the four electron withdrawing fluorine substituents on the *H*$_2$BDC organic linker.[24,25] The deterioration in the degree of crystallization is even more pronounced in the case of the trimellitic acid *H*$_2$BDC-COOH. This trend, which has been already reported in the literature for the functionalized UiO-66-COOH,[26] can be associated with the occurrence of a structural distortion or loss of symmetry in the UiO-66-type framework due to the presence of a third additional carboxylic acid group (in the position 2), also capable of metal coordination. The change in the conformation of the linker may dramatically influence the directionality of the coordination bonds between the carboxylate groups and Zr(IV) metal centers during the crystal growth. Another explanation could come from the lower pKa value of trimellitic acid as compared to other derivatives such as 2-aminoterephatalic acid.[27] Besides, it can be mentioned that, when the *H*$_2$BDC-COOH organic linker is mixed in the presence of increasing amounts of α-CD during the synthesis, more poorly defined materials are systematically obtained, as evidenced from the XRD patterns of the UiO-66-COOH (Figure S16, ESI). In this particular case, a partial inclusion complex between the α-CD and trimellitic acid linker that would exert more steric hindrance around the COOH groups and prevent crystallization from occurring, cannot be excluded. As evidenced by our ^{1}H NMR studies in aqueous solution, supramolecular interactions of α-CD with *H*$_2$BDC-COOH have been confirmed (1D and T-ROESY). For instance, the ^{1}H NMR spectrum of a stoichiometric mixture of α-CD/*H*$_2$BDC-COOH mixture shows that the most significant variations in the chemical shifts for the α-CD protons are observed for the internal protons, H-3 and H-5, located inside the hydrophobic cavity (Figure 4-A). The fact that the magnitude of the shielding effect is larger on the H-3 proton with respect to H-5 suggests that the BDC aromatic ring preferentially penetrates through the secondary face of the α-CD torus. This assumption is further confirmed by a T-ROESY experiment (Figure 4-B). Thus, the cross-peaks between the aromatic protons of *H*$_2$BDC-COOH and the H-3 and H-5 protons of α-CD are indicative of a shallow inclusion.

Fourier-Transform Infrared Spectroscopy (FTIR) was also employed to confirm the integrity of the different UiO-66-R MOF structures, and the corresponding spectra are collected in Figure 5. The FTIR spectra undergo only very small variations, indicating that the vibrational structure is little affected by the nature of the dicarboxylic acid linker used. Thus, the C-O asymmetric and symmetric stretching of the carboxylate groups can be readily detected on each of the samples, as evidenced by strong intense bands in the range of 1580-1600 cm^{-1} and 1380-1400 cm^{-1}, respectively.[28,29] Another set of characteristic absorption bands at ca. 1340, 1500 and 1650 cm^{-1} are assigned to the C=C stretching modes of the aromatic BDC rings. Note that, in the case of the UiO-66-PDC MOF, the 2,5-pyridine dicarboxylic acid linker exhibits a stretching vibration band at 1600 cm^{-1} corresponding to C=N in the pyridine ring. The presence of the different functional groups attached to *H*$_2$BDC can also be identified. Thus, the peak at 1257 cm^{-1} corresponds to the C-N stretching of the aromatic amine on UiO-66-NH_2 while that at 1235 cm^{-1} is attributed to the C-O stretching of the aromatic alcohol on UiO-66-$(OH)_2$. For the UiO-66-COOH and UiO-66-$(COOH)_2$ synthesized from the trimellitic and pyromellitic acids, respectively, the presence of remaining protonated carboxylic groups on the aromatic ring is characterized by the appearance of an additional stretching band in the range between 1710 and 1720 cm^{-1}. Analysis of the FTIR spectrum of UiO-66-NO_2 reveals two bands at ca. 1544 and 1347 cm^{-1}, which can be assigned to the vibrational modes of the stretching vibrations of pendant NO_2 groups. In the FTIR spectra of UiO-66-Br and UiO-66-F_4, it is also possible to distinguish characteristic bands of the halogen substituents: the C-Br stretching vibration of medium intensity at 730 cm^{-1} and the strong C-F stretching absorption at 996 cm^{-1}. It should be noted that, regardless of the amount of α-CD, the FTIR spectra do not show any vibration bands assignable to C-O-H bending modes of cyclodextrins, which are known to strongly contribute to the absorption features in the spectral range between 1000 and 1300 cm^{-1}.[30] The absence of cyclodextrin moieties indicates that they have been efficiently eliminated removed during the washing step.

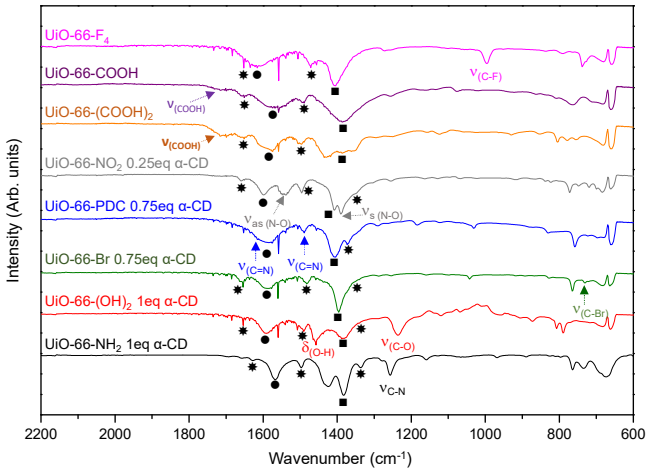

Figure 5. FTIR spectra in the 600-2200 cm^{-1} region for the selected UiO-66-R materials synthesized using various amounts of α-CD. from the bottom to the top UiO-66-NH_2 1 eq. α-CD (black), UiO-66-$(OH)_2$ 1 eq. α -CD (red), UiO-66-Br 0.75 eq. α-CD (green), UiO-66-PDC 0.75 eq. α-CD (blue), UiO-66-NO_2 0.25 eq. α-CD (grey), UiO-66-$(COOH)_2$ (orange), UiO-66-COOH (purple) and UiO-66-F_4 (pink). The star, circle and square symbols refer to aromatic C=C stretching modes, C-O asymmetric and symmetric stretching modes of carboxylates groups, each ot them associated with the DCA linker.

As a complement to FTIR analyses, and in order check that the number of carbohydrate residues within the porous frameworks was always negligible, the UiO-66-type MOFs synthesized with different linkers have been subjected to digestion experiments in alkaline solutions. Briefly, a precise mass of Zr-MOF is immersed in a NaOH/D_2O solution followed by an ultrasonic treatment at room temperature. The ^1H NMR spectra of the transparent supernatant solutions after alkaline degradation are given in Figure 6.

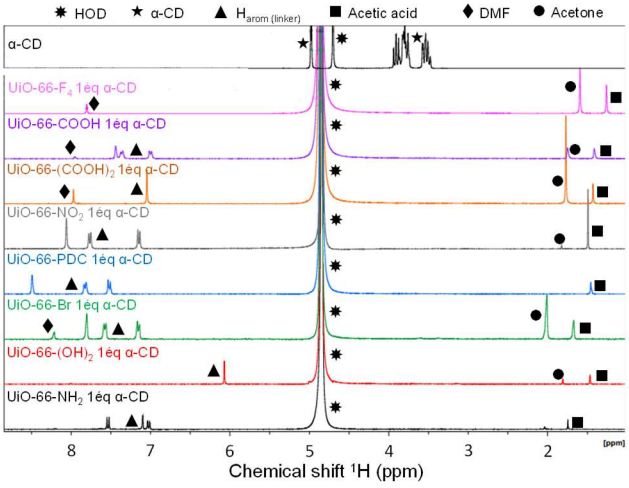

Figure 6. 1H NMR spectra in D_2O at 25 °C of α-CD, and compounds resulting from digestion by NaOH of UiO-66-R synthesized with 1 equivalent of α-CD with respect to the organic linker.

To facilitate comparison, the results presented have been obtained from digested samples of UiO-66-R MOFs prepared using a 1:1 α-CD:linker molar ratio. Such a high ratio has been selected to try to incorporate the α-CD in the MOF frameworks, if possible. The control ^1H NMR spectrum of α-CD has also been added for comparison. Thus, we observe that the NMR spectra data for the digested samples contain, in addition to the resonances attributed to the aromatic protons of the deprotonated H_2BDC linkers (δ ~ 7-8 ppm), additional singlet signals at around δ ~2 ppm. These peaks indicate the presence of acetate residues and must be related to the coordinating modulator effect of acetic acid, which can be covalently attached to crystalline structure. Besides, the absence of any resonance near 3–4 ppm corresponding to the cyclodextrin structure denotes also that there is no chemical bonding or strong interaction bonding during the MOF synthesis. This is consistent with the results of FTIR spectroscopy and supports the fact that the α-CD may, depending on the chemical nature of the organic linker, influence the crystallization process, but without being incorporated into the metal-organic framework.

Thermogravimetric (TG) analyses were further performed to examine the thermal stability of the different UiO-66-R materials in the temperature range from 100°C to 800°C (Figure 7).

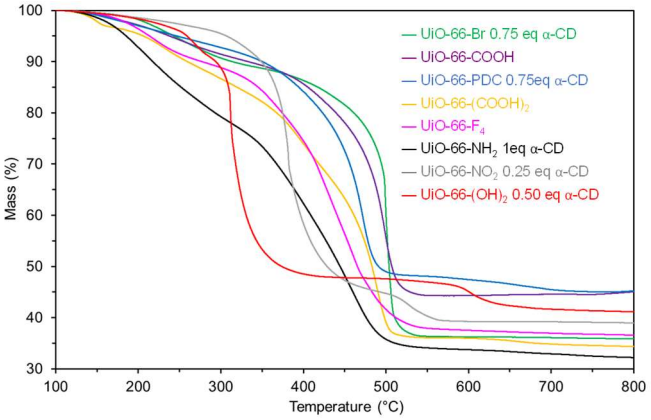

Figure 7. TG profiles of selected UiO-66-R materials synthesized using various amounts of α-CD. UiO-66-NH_2 1 eq. α-CD (black), UiO-66-$(COOH)_2$ (orange), UiO-66-Br 0.75 eq. α-CD (green), UiO-66-F_4 (pink), UiO-66-NO_2 0.25 eq. α-CD (grey), UiO-66-$(OH)_2$ 1 eq. α-CD (red), UiO-66-COOH (purple), UiO-66-PDC 0.75 eq. α-CD (blue).

As indicated in the experimental section in ESI, UiO-66-R samples were thermally treated in a first stage in the TG equipment at 100°C for 2 h in order to estimate the moisture content present inside the porous framework. This initial drying step is typically characterized by a weight loss in the low temperature region (T < 100°C) associated with the removal of physically adsorbed water and trapped cleaning solvents (DMF and/or methanol). We observe that all UiO-66-R prepared with the different organic linkers, with or without α-CD, contain approximately 10−20 wt. % of guest solvent molecules in the cavities, in line with the nature of these structured porous materials. Once the temperature exceeds 100°C, the TG profiles show that the decomposition process of UiO-66 type MOFs begins, with the appearance of two distinct weight loss regions. The first weight loss, associated with the rather slow dehydroxylation process of the inorganic Zr_6 oxo-clusters, takes place between 150 and 350°C. The second weight loss occurring in the temperature range 350–550°C for most samples, is more rapid and abrupt. It corresponds to the decomposition of the

organic linker, and consequently leads to the complete breakdown of the structure network. The variation in weight loss (from 40 to 55 %) can be partly explained by differences in the molecular weights of the linker. It must also be noted that the thermal stability of the UiO-66-R materials is affected to different extents depending on the nature of the dicarboxylate compound employed. Besides, the temperature for which the decomposition rate is as its maximum (T_{max}) can be identified with the aid of DTG curves. Thus, the impact of the organic linker on UiO-66-R thermal stability can be ranked as follows: UiO-66-Br (T_{max} = 500°C) > UiO-66-COOH (T_{max} = 498°C) > UiO-66-$(COOH)_2$ (T_{max} = 490°C) > UiO-66-PDC (T_{max} = 472°C) > UiO-66-F_4 (T_{max} = 461°C) > UiO-66-NH_2 (T_{max} = 460°C) > UiO-66-NO_2 (T_{max} = 381°C) > UiO-66-$(OH)_2$ (T_{max} = 312°C). Except for the UiO-66-$(OH)_2$, for which the decomposition temperature seems to be abnormally low, all other materials retain high thermal stability, even with the functional groups present at the linker units, such as COOH or F. This trend, which is in good agreement with some previously published results,[21,31,32] is generally attributed to the strong interactions between the carboxylates and the inorganic bricks. It is also worth mentioning that, irrespective of the ratio of α-CD to linker introduced during the synthesis, almost superimposable TG profiles are obtained considering the same series of UiO-66-R MOF (Figure S18-S25, ESI). This is in line with the hypothesis that CDs do not create defects within the MOF structure but rather affect the MOF surface by generating of dangling linkers. Nevertheless, the relationship between MOF precursors and stability features is not straightforward. During the decomposition process of UiO-66 derivatives, several different effects could be simultaneously involved, such as steric and electronic factors as well as intrinsic thermal characteristics of organic linkers, which makes correlation difficult.[21] It is interesting to note that the UiO-66-Br has a slightly higher thermal resistance, which can be related to known flame retardant properties of numerous organobrominated compounds.

Taken together, the above characterization results for UiO-66-R materials have demonstrated that the utilization of α-CD, in well-defined concentration ranges, could promote the formation of some UiO-66-R MOFs with superior textural properties. However, the impact α-CD is more or less positive depending on the type of organic linker. The most significant effects were observed in the UiO-66-R series with R = NH_2, $(OH)_2$, Br, PDC and NO_2 while the effects were minor or indiscernible in the remaining members of the series. The first question that arises is whether the complexation ability of this cyclic oligosaccharide can interfere with the MOF crystal growth processes, by regulating the coordination environment of the linker with the Zr-inorganic brick. It is well-known that the internal cavity of cyclodextrins, which is hydrophobic, can accommodate a wide range of guest molecules of appropriate size and shape. Regarding the dimensions of α-CD (internal diameter = 0.47–0.53 nm), the possibility can be excluded that α-CD interacts with the Zr_6-clusters (Ø ~ 1.1 nm) in the form of inclusion complex, but not with smaller molecules that are aromatic carboxylic acid linkers. Thus, the inclusion ability of α-CD towards the eight different linker derivatives deserved to be examined separately. Aqueous solutions of H_2BDC-R or H_2PDC mixed with α-CD (in a 1:2 molar ratio) have been studied by ^{1}H NMR (1D and 2D-T-ROESY) (Figures S26-S40, ESI). NMR results have revealed contrasted results in terms of recognition behavior of α-CD towards aromatic dicarboxylic acid molecules. The ^{1}H NMR spectra of α-CD in mixture with compounds, such as H_2BDC-Br (Figure S30, ESI), H_2 PDC (Figure S32, ESI), H_2BDC-NO_2 (Figure S34, ESI) and H_2BDC-COOH (Figure S38, ESI) have shown tiny, but significant chemical shifts, involving mainly the secondary face protons H-3 ($\Delta\delta \approx 0.11$ -0.34 ppm). In line with this, T-ROESY coupling cross peaks were also detected, indicative of the formation of shallow inclusion complexes with these guests (Figures S31, S33, S35 and S39, ESI). In contrast with the other four linkers [with R = NH_2, $(OH)_2$, $(COOH)_2$ and F_4], no clear chemical shift changes of the proton signals assigned to the α-CD could be evidenced in the ^{1}H NMR spectra, reflecting the absence of supramolecular interactions (Figures S26, S28, S36, S40, ESI). This is also confirmed by NMR T-ROESY experiments which do not reveal signs of cross-peaks (Figures S27, S29, S37, ESI). From these NMR results, it is now evident that the variations of the specific surface area versus amount of α-CD are not driven by the host-guest complexation, presumably because the interactions are too weak to influence the coordination of the linkers to the metal nodes, and therefore crystal nucleation and growth.

Another factor that may be involved in determining the discrepancy effect of α-CD in the hydrothermal synthesis of UiO-66-type MOFs is the water solubility of the ditopic linkers. Indeed, some previous studies have established that the linker availability could be an essential parameter for the efficient hydrothermal synthesis of UiO-66 derivatives. [7] The availability of the linker can be enhanced by increasing the initial concentration or adjusting the pH in order to assist the deprotonation and coordination of the carboxylate linkers on the Zr_6 oxo clusters.[9]

Based on the above assumption, the water solubility of the series of dicarboxylic acids studied has been experimentally determined by an isothermal saturation method at 25°C. The corresponding solubility values are given in Table 2, as well as the synthesis yields and BET specific surface areas obtained for each UiO-66-R, prepared both without and with optimized amount of α-CD.

The organic linkers can be categorized into two main groups. The first one includes the slightly and moderately soluble organic linkers having a water solubility of less than or equal to 5 g L^{-1} (Table 2, entries 1-5). The second one consists of linkers, which have a good solubility in water, typically above 10 g L^{-1} (Table 2, entries 6-8).

It can be suggested from the solubility trend that the choice of the linker is critical for producing UiO-66-R materials with enhanced specific surface areas, when using α-CD. We observe an overall trend of decreasing the optimum amount of cyclodextrin used with an increase in water solubility. For instance, the number of α-CD per mole of linker ranges from 1 for H_2BDC-NH_2 (0.2 g L^{-1}) and H_2BDC-$(OH)_2$ (0.35 g L^{-1}) to a minimum of only 0.25 for H_2BDC-NO_2 (5 g L^{-1}).

Table 2. Estimated water solubility of each organic linker and comparison of the percentage synthesis yield and BET specific surface area of hydrothermally synthesized UiO-66-R derivatives prepared without and with the optimized amount of α-CD with respect to the dicarboxylic acid linker.

Entry	MOF UiO-66-R	Linker solubility (g L^{-1})	Yield (%)		BET surface area (m^2 g^{-1})	
			without CD	with α-CD[a]	without CD	with α-CD[a]
1	UiO-66-NH_2	0.20	95	51 (1 eq α-CD)	611	1451 (1 eq α-CD)
2	UiO-66-$(OH)_2$	0.35	70	55 (1 eq α-CD)	689	893(1 eq α-CD)
3	UiO-66-Br	0.80	89	93 (0.75 eq α-CD)	763	862 (0.75 eq α-CD)
4	UiO-66-PDC	1.6	70	84 (0.75 eq α-CD)	468	974 (0.75 eq α-CD)
5	UiO-66-NO_2	5.0	47	57 (0.25 eq α-CD)	592	713 (0.25 eq α-CD)
6	UiO-66-$(COOH)_2$	10	83	89[b]	391	405[b]
7	UiO-66-COOH	14	72	62[b]	102	89[b]
8	UiO-66-F_4	26	76	73[b]	383	363[b]

[a] The number in brackets indicates the molar ratio of the added α-CD under the optimum conditions for the highest specific surface area. [b] The result refers to a molar ratio of α-CD to linker of 0.5, this ratio being arbitrary selected as an intermediate and representative value to highlight the lack of effect of α-CD during the MOF preparation. It roughly corresponds to the average results obtained with the four experimental molar ratios, which varied from 0.25 to 1.

As previously evidenced by ^{1}H NMR, pure host-guest inclusion complexes cannot account for the role of α-CD. Instead, it can be suggested that an effect of dispersion on the insoluble linker aggregates could contribute to a significant extent to the improvement of the MOF synthesis process, which by definition occurs in a complex heterogeneous environment with critical dynamics, as the MOF particle grow larger. The complexity is worsened by the fact that high weight concentrations of linker are used in the beginning of the syntheses (typically between 17 and 25 g L^{-1}), justifying the presence of linker aggregates in saturated solutions. In fact, such a dispersion effect has been nicely evidenced for UiO-66-NH_2 and the mechanism of this phenomenon has been associated with the adsorption of α-CD on hydrophobic linker aggregates.[15] This suggests that α-CD, in combination with acetic acid, is implicated in the regulation of MOF particle formation and growth rate, in agreement with the concept of modulated synthesis. However, when the solubility of the linker is increased, the effect on the dispersion is expected to be less important, possibly explaining why the relative amount of α-CD necessary for obtaining the optimized porous network structure is significantly reduced. In the case of H_2BDC-$(COOH)_2$, H_2BDC-COOH and H_2BDC-F_4 as linkers, the solubility is so high (10, 14 and 26 g L^{-1}, respectively) that the role of α-CD as co-modulator for the growth of MOF crystallites appears to be negligible.

Regarding the yields of the synthesis of the different UiO-66-R, it can be noticed that, without α-CD, the values are relatively high, overall ranging from 70 to 95 %. The only exception is UiO-66-NO_2 that exhibits a significant lower yield of 47 % with respect to the other materials. This observation suggests that our experimental conditions are not yet optimized and, would require further improvement. Nevertheless, to our knowledge, the use of H_2BDC-NO_2 as the bridging ligand has been the subject of only one study under hydrothermal conditions, thus making the comparison difficult.[33] Under controlled conditions of α-CD, we observe that the synthesis yields are affected to different extents depending on the nature of the organic linker employed. Indeed, while the materials prepared with H_2BDC-Br, H_2PDC and H_2BDC-NO_2 reveal more or less significant increases in yield (from 4% to 14%), the yield for the UiO-66-type materials synthesized using H_2BDC-NH_2 and H_2BDC-$(OH)_2$ in the presence of 1 equivalent of α-CD dramatically drops by 44 % and 25 %, respectively. This behavior observed with the two least soluble linkers can be explained by difficulties in recovering the solid particles at the end of the synthesis owing to the presence of a larger number of small-size particles remaining dispersed in the reaction medium or being lost during rinsing steps.

The overall results presented in this work provide a fundamental basis to synthesize, through cyclodextrin-assisted modulated synthesis, UiO-66 MOF derivatives based on the combination of two different components: the oxo-Zr_6 clusters as the inorganic bricks and the dicarboxylic aromatic acids as the bridging ligands. Thus, the α-CD may have a remarkable positive impact on the specific surface areas of the MOF synthesized. The magnitude of the impact is dependent on several factors, such as the number of molar equivalents of α-CD introduced during the synthesis and the water solubility of the organic linker.

In particular from Figure 8, it can be seen there exists an interplay between the decrease in solubility of the organic linker and the increase in BET specific surface area of the resulting UiO-66 MOF. Typically, when the solubility of the linker is low (less than or equal to 5 g L^{-1}), the corresponding BET surface areas show an uptrend (from 13 % to 137 %) with the use of well-defined amounts of α-CD. Conversely, when the solubility exceeds this range (above 10 g L^{-1}), the cyclodextrin effect tends to become negligible or extremely limited, since the hydrophilic properties of the linkers

[i.e. H_2BDC-$(COOH)_2$, H_2BDC-COOH and H_2BDC-F_4] are already dominant in the aqueous media. Such a behavior gives an insight that the hydrophobic-hydrophilic balance in water solutions of α-CD plays an important role in the structural-functional organizations and regulation mechanisms during the growth of UiO-66 solid particles.

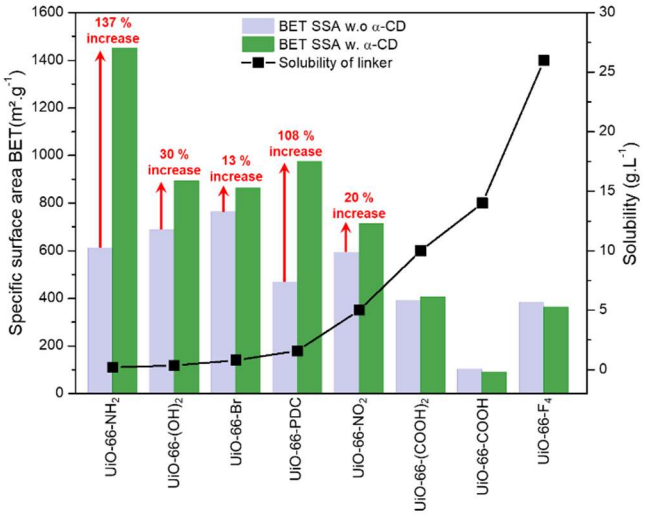

Figure 8. Relationship between BET specific surface area and water solubility of the dicarboxylic acid linker of UiO-66-type MOFs prepared under hydrothermal conditions, without or with the optimized amount of cyclodextrins. For UiO-66-$(COOH)_2$, UiO-66-COOH and UiO-66-F_4, the results with α-CD refer to 0.5 equivalents of α-CD with respect to the ligand, this ratio being arbitrary selected as an intermediate and representative value. (see Table 2 for more detail).

By comparing these results to previously reported UiO-66 MOF derivatives, where the reactions took place under solvothermal conditions, our cyclodextrin-assisted synthetic approach allows to obtain UiO-66-R MOF materials with comparable textural properties (or even superior) in such aqueous environments, as evidenced in the case of UiO-66-NH_2, UiO-66-$(OH)_2$, UiO-66-Br and UiO-66-NO_2 (Table 3). For example, the BET surface areas of UiO-66-NH_2 has been increased from the reported value of 1200 to 1451 $m^2 \cdot g^{-1}$ (~20 % increase). It is also noteworthy that, to the best of our knowledge, it is the first time that the hydrothermal synthesis is applied for the synthesis of UiO-66-Br Zr-MOF materials with 2-bromoterephthalate as the linker, and affording a high BET specific (862 $m^2 \cdot g^{-1}$). For other UiO-66 analogues, such as UiO-66-PDC, the results offer a mixed picture. Thus, even if the specific area of UiO-66-PDC was multiplied by a factor of 2 in the presence of 0.75 equivalent of α-CD with respect to the linker, the highest BET surface area was found to be only 974 $m^2 \cdot g^{-1}$, which is significantly lower than what was previously measured on a hydrothermally prepared UiO-66-PDC sample in the literature (1380 $m^2\ g^{-1}$). This discrepancy could be attributed to differences in the experimental procedure, in terms of temperature (120°C) and modulation conditions (formic acid:H_2O 9:1).

Finally, the synthetic methodology of UiO-66 derivatives based on the use of α-CD as co-modulator, can be seen as a versatile innovative method that could provide a suitable aqueous reaction environment, mimicking the behavior of organic solvents in close proximity of the construction sites of Zr-based MOF structures. This behavior can be explained by the fact that α-CD act as a hydrotropic structure, containing both hydrophilic and hydrophobic parts. Indeed, the spatial distribution of hydroxyl functions towards the outside of the torus confer to the CD molecule a hydrophilic character while the presence of non-polar functions -CH_2- towards the interior makes the cyclodextrin cavity hydrophobic.

Table 3. BET surface area of the best reported UiO-66-type MOFs synthesized by solvothermal synthesis, and this work.

MOF UiO-66-R	BET specific surface area ($m^2\ g^{-1}$)	
	Solvothermal conditions	*This work*
UiO-66-NH_2	1200 [34]	1451 (1 eq α-CD)
UiO-66-$(OH)_2$	814 [35]	893 (1 eq α-CD)
UiO-66-Br	784 [36]	862 (0.75 eq α-CD)
UiO-66-PDC	- [a] [b] (1380) [31]	974 (0.75 eq α-CD)
UiO-66-NO_2	729 [35]	713 (0.25 eq α-CD)
UiO-66-$(COOH)_2$	221 [35]	391
UiO-66-COOH	842 [37]	102
UiO-66-F_4	- [a] [b] (833) [14]	383

[a] no value reported in the literature under solvothermal conditions. [b] The value in bracket refers to the BET area for a UiO-66-R material prepared under hydrothermal conditions.

Conclusion

In this work, we investigated the possibility of using α-cyclodextrin as the co-modulator agent for the hydrothermal synthesis of a series of UiO-66 Zr-based MOFs with controlled crystalline frameworks and porosities. A variety of substituted benzene-1,4-dicarboxylic acids and pyridine-2,5-dicarboxylic acid was selected as representative ditopic carboxylate linkers. For most of the dicarboxylic aromatic acid linkers, the addition of an optimum amount of α-CD to the Zr_6-oxo-clusters could advantageously enhance the textural properties of the resulting UiO-66-R MOFs, and in particular their BET surface areas. This procedure was shown to be particularly effective when the linkers are poorly soluble in water (typically less than or equal to 5 g L^{-1}). In this case, we found out that simple adjustments of the molar ratio of α-CD to linker to synthesis during the synthesis could lead to pure UiO-66 phases, exhibiting porosities similar to those obtained through conventional solvothermal methods, as confirmed by XRD and N_2 sorption analysis. Besides, we reported for the first time that UiO-66 Br could be successfully synthesized from this cyclodextrin-assisted hydrothermal method. Through this co-modulated synthesis method, α-CD could exert fine control upon the growth of the metal–organic frameworks by competitive metal coordination but also, facilitating the dispersion of the poorly water-soluble linkers and subsequent attachment to the zirconium

nodes. This method, which has the advantages of being simple and environmentally friendly, should provide new opportunities for the development of other types of metal-organic frameworks.

Experimental Section

Chemicals: All solvents and reagents were commercially purchased and used as received without further purification. Zirconium (IV) oxychloride octahydrate ($ZrOCl_2 \cdot 8H_2O$, 99.5%), *N,N*-dimethylformamide (DMF, 99.8%) were purchased from Sigma-Aldrich (Quentin-Fallavier, France). Substituted terephthalic acids (H_2BDC-R, purity > 99%) and 2,5-pyridine dicarboxylic acid (H_2PDC, purity > 99%) were purchased from Acros Organics - Fisher Scientific France (Illkirch, France) or Strem Chemicals (Bischheim, France). Acetic acid was provided by Fisher Scientific while absolute methanol and ethanol were purchased from Verbiese (Merville, France).

Modulated hydrothermal synthesis of UiO-66-R: $ZrOCl_2 \cdot 8H_2O$ (0.322 g, 1 mmol) was first dissolved in a mixture of water/acetic acid (5 mL/5 mL). In a second step, the diacid derivative (1 mmol) and the α-CD were previously ground in a laboratory-scale ball-mill (Retsch MM400), equipped with a 10 mL zirconia grinding jar containing zirconia balls (diameter of 9 mm). The grinding jars were horizontally shaken at an oscillation frequency of 30 Hz for 10 minutes. Then, the solid-phase mixture was added to the acidic solution of the zirconium salt. The reaction mixture was further heated at 90 °C for 24 h. The precipitate was washed successively with DMF (2 × 10 mL), water (2 × 10 mL) and methanol (2 × 10 mL) in order to remove residual reagents from the MOF pores. In a final step, the sample was dried under vacuum at 100 °C for 24 h to yield the final UiO-66-R product

Digestion experiments under alkaline conditions: Digestion experiments were carried out and monitored by 1H NMR as follows: NH_2-UiO-66 (10 mg) and D_2O (600 μL) were introduced in a NMR tube. Sodium hydroxide (60 mg) was then added and the resultant solution was placed in an ultrasonic bath at room temperature for 5 minutes to provoke the MOF digestion.

Determination of the water solubility of linkers: A saturated water solution (20 mL) of dicarboxylic acid derivative [H_2BDC-R or H_2PDC] was stirred at 25°C during 30 minutes. The suspension was filtered. Then NaOH (0.1 M) was added to 10 mL of the filtrate and the amount of excess NaOH was determined by back-titration with HCl (0.1 M). The water solubility of the dicarboxylic acid linker was the calculated by the following formula:

$$\text{Linker solubility (g L}^{-1}) = \frac{(C_{NaOH} \times V_{NaOH} - C_{HCl} \times V_{eq}) \times MW_{DCA}}{2 \times V_{DCA}}$$

where MW_{DCA} is the molecular weight of the dicarboxylic acid linker derivative, V_{DCA} corresponds to the volume of filtrate and, Veq is the equivalence point. Average values of water solubility were obtained from at least two measurements.

Characterization methods: N_2 sorption isotherms were collected at -196°C using an adsorption analyzer Micromeritics Tristar II 3020. Prior to analysis, 80-100 mg of a freshly dried sample (100°C, overnight) was degassed for 2 hours at 100°C under vacuum. For the surface area determinations, the Langmuir and Brunauer-Emmett-Teller (BET) models were applied to fit the experimental data. The BET specific surface areas were determined in the P/P^0 range from 0.001 to 0.05, identified by applying the four consistency criteria developed by Rouquerol et *al.* [Erreur ! Signet non défini.]: (i) the BET C constant should be positive; (ii) the function V(1- (P/P°)) should continuously increase with P/P°; (iii) the monolayer capacity (V_m) should correspond to a relative pressure P/P° included within the selected pressure; (iv) the calculated value for monolayer formation ($1/(\sqrt{C} + 1)$) should be approximately equal to P/P° at the monolayer formation (a tolerance of 20% has been accepted). In all cases, the four consistency criteria were satisfactorily fulfilled. The t-plot method was used to estimate the amount of micropores based on the Halsey thickness equation. The total pore volumes were estimated from the adsorbed amounts at a relative pressure of ca. 0.95. Based on the N_2 adsorption data, a nonlocal density functional theory (NLDFT) model included in the commercial Tristar II 3020 V1.03 software was used for the calculation of pore size distributions (assuming slit pore geometry). X-Ray Diffraction (XRD) measurements were performed using a Rigaku ULTIMA IV diffractometer equipped with a Cu anticathode (Kα = 1.5418 Å), Soller slits to limit the divergence of X-ray beam and a nickel foil filter to attenuate the Cu Kβ line. XRD patterns were recorded in the 2θ range of 3-50° (scan speed of 0.4° min^{-1}) using the Bragg-Brentano configuration. Fourier transform infrared (FT-IR) experiments were performed using a Spectrum Two Perkin-Elmer FT-IR spectrometer equipped with a single-reflection diamond module (ATR) and a deuterated triglycine sulfate detector. FTIR spectra were recorded in the wavenumber range of 400−4000 cm^{-1}. ^{1}H NMR spectra were recorded on a 300 MHz Bruker Avance III HD spectrometer using D_2O (99.92% isotopic purity, Eurisotop) as a solvent. The 2D T-ROESY experiments were run using the software supplied by Bruker. Mixing times for T-ROESY experiments were set at 300 ms. The data matrix for the T-ROESY was made of 512 free induction decays, 1 K points each, resulting from the co-addition of 32 scans. The real resolution was 1.5–6.0 Hz/point in F2 and F1 dimensions, respectively. They were transformed in the non-phase-sensitive mode after QSINE window processing. TG analyses were performed using a Mettler Toledo TGA/DSC 3+ Start System instrument equipped with a flow gas system. The heat treatment schedule included 2 successive stages as follows: a first heating is applied up to 100°C for 120 min (drying stage), immediately followed by a second heating from 100°C to 800°C (decomposition stage). In all experiments, the sample weight was about 10 mg while the gas flow (air) and heating rate were 50 mL min^{-1} and 5°C min^{-1}, respectively. The moisture percentage was calculated by the weight loss after 120 minutes at 100°C while the remaining mass percentage was calculated according to the following formula: mass (%) = 100 x (m)/m_0 where m_0 is the initial dry mass of the MOF sample stabilized at 100°C.

Acknowledgements

The authors acknowledge the Chevreul Institute (FR 2638), Ministère de l'Enseignement Supérieur et de la Recherche, Région Hauts de France and FEDER program for supporting and partially funding this work. Guillaume Hoyez is grateful to the University of Artois for the funding of his PhD grant. Dr. Jérémy Ternel (UCCS, University of Artois) for NMR analyses and Dr. Nicolas Kania (UCCS, University of Artois) for TGA measurements.

Keywords: Cyclodextrins • Co-modulator • Hydrothermal synthesis • Metal-organic frameworks • Zirconium

[1] a) R. S. Forgan, R. A. Smaldone, J. J. Gassensmith, H. Furukawa, D. B. Cordes, Q. Li, C. E. Wilmer, Y. Y. Botros, R. Q. Snurr, A. M. Z. Slawin, J. Fraser Stoddart, *J. Am. Chem. Soc.* **2012**, *134*, 404-417; b) V. V Butova, M. A. Soldatov, A. A. Guda, K. A. Lomachenko, C. Lamberti, *Russ. Chem. Rev.* **2016**, *85*, 280-307; c) S. Yuan, J-S. Qin, C. T. Lollar, H-C. Zhou, *ACS Cent. Sci.* **2018**,*4*, 440-450; d) S. Yuan, L. Feng, K. Wang, J. Pang, M. Bosch, C. Lollar, Y. Sun, J. Qin, X. Yang, P. Zhang, Q. Wang, L. Zou, Y. Zhang, L. Zhang, Y. Fang, J. Li, H-C. Zhou, *Adv. Mater.* **2018**, *37*, 1704343; e) S. Fordham, X. Wang, M. Bosch, H-C. Zhou in *Lanthanide Metal-Organic Frameworks. Structure and Bonding,* Vol 163 (Eds.: P. Cheng), Springer, Berlin, 2014, pp. 1-27.

[2] H. Furukawa, K. E. Cordova, M. O'Keeffe, O. M. Yaghi, *Science* **2013**, *341*, 1230444.

[3] a) X. Zhang, X. Shi, J. Chen, Y. Yang, G. Lu, *J. Environ. Chem. Eng.* **2019**, *7*, 103405-103413; b) J. Heine, K. Müller-Buschbaum, *Chem. Soc. Rev.* **2013**, *42*, 9232-9242; c) I. Abánades Lázaro, R. S. Forgan, *Coord. Chem. Rev.* **2019**, *380*, 230-259; d) A. Dhakshinamoorthy, A. Santiago-Portillo, A. M. Asiri, H. Garcia, *ChemCatChem* **2019**, *11*, 899-923.

[4] a) Z. Hu, D. Zhao, *Dalton Trans.* **2015**, *44*, 19018-19040; b) A. Kirchon, L. Feng, H. Drake, E. A. Joseph, H-C. Zhou, *Chem. Soc. Rev.* **2018**, 47, 8611-8638; c) Q. Wang, D. Astruc, *Chem. Rev*. **2020**, *120*, 1438–1511.

[5] Y. Bai, Y. Dou, L.-H. Xie, W. Rutledge, J.-R. Li, H.-C. Zhou, *Chem. Soc. Rev.* **2016**, *45*,. 2327-2367.

[6] J. H. Cavka, S. Jakobsen, U. Olsbye, N. Guillou, C. Lamberti, S. Bordiga, K. P. Lillerud, *J. Am. Chem. Soc.* **2008**, *130*, 13850-13851.

[7] D. Morelli Venturi, F. Campana, F. Marmottini, F. Costantino L. Vaccaro, *ACS Sustainable Chem. Eng.* **2020**, *8*, 17154-17164.

[8] H. Reinsch, B. Bueken, F. Vermoortele, I. Stassen, A. Lieb, K. P. Lillerud, D. De Vos, *CrystEngComm* **2015**, *17*, 4070-4074.

[9] L. Huelsenbeck, H. Luo, P. Verma, J. Dane, R. Ho, E. Beyer, H. Hall, G. M. Geise, G. Giri, *Cryst. Growth Des.* **2020**, *20*, 6787-6795.

[10] Z. Ni, R. I. Masel, *J. Am. Chem. Soc.* **2006**, *128*, 12394-12395.

[11] a) K. Užarević, T. C. Wang, S. Y. Moon, A. M. Fidelli, J. T. Hupp, O. K. Farha, T. Friscić, T. *Chem. Commun.* **2016**, *52*, 2133-2136; b) A. M. Fidelli, B. Karadeniz, A. J. Howarth, I. Huskić, L. S. Germann, I. Halasz, M. Etter, S.-Y. Moon, R. E. Dinnebier, V. Stilinović, O. K. Farha, T. Friščić, K. Užarević, *Chem.Commun*. **2018**, *54*, 6999-7002; c) D. Prochowicz, J. Nawrocki, M. Terlecki, W. Marynowski, J. Lewiński, *Inorg. Chem.* **2018**, *57*, 13437-13442.

[12] M. Faustini, J. Kim, G.-Y. Jeong, J. Y. Kim, H. R. Moon, W.-S. Ahn, D.-P. Kim, *J. Am. Chem. Soc.* **2013**, *39*, 14619-14626.

[13] I. Pakamorė, J. Rousseau, C. Rousseau, E. Monflier, P. Ágota Szilágyi, *Green Chem.* **2018**, *20*, 5292-5298.

[14] Z. Hu, Y. Peng, Z. Kang, Y. Qian, D. Zhao, *Inorg. Chem*. **2015**, *54*, 4862-4868.

[15] G. Hoyez, J. Rousseau, C. Rousseau, S. Saitzek, J. King, P. Ágota Szilágyi, C. Volkringer, T. Loiseau, F. Hapiot, E. Monflier, A Ponchel, *CrystEngComm* **2021**, *23*, 2764-2772.

[16] D. Prochowicz, A. Kornowicz, J. Lewiński, *Chem. Rev*. **2017**, *117*, 13461–13501.

[17] J. Rouquerol, P. Llewellyn, F. Rouquerol, *Stud. Surf. Sci. Catal*. **2007**, 160, 40-56.

[18] H. Wu Y. S. Chua, V. Krungleviciute, M. T. Ping Chen, T. Yildirim,W. Zhou, *J. Am. Chem. Soc*. **2013**, *28*, 10525-10532.

[19] P. Xydias, I. Spanopoulos, E. Klontzas, G. E. Froudakis, P. N. Trikalitis, *Inorg. Chem.* **2014**, *53*, 679-681.

[20] I. V Terekhova, R. S. Kumeev, G. A. Alper, *J. Incl. Phenom. Macrocycl. Chem.* **2008**, *62*, 363-370.

[21] M. Kandiah, M. Hellner Nilsen, S. Usseglio, S. Jakobsen, U. Olsbye, M. Tilset, C. Larabi, E. A. Quadrelli, F. Bonino, K. P. Lillerud, *Chem. Mater*. **2010**, *22*, 6632-6640.

[22] N. Terinte, R. Ibbett, K. C Schuster*, Lenzinger Ber*. **2011**, *89*, 118-131.

[23] M. J. Cliffe, W. Wan, X. Zou, P. A. Chater, A. K. Kleppe, M. G. Tucker, H. Wilhelm, N. P. Funnell, F.-X. Coudert, A. L. Goodwin, *Nat. Commun*. **2014**, *5*, 4176.

[24] M. Kalaj, K. E. Prosser S. M. Cohen, *Dalton Trans.* **2020**, *49*, 8841-8845.

[25] Z. Chen, X. Wang, H. Noh, G. Ayoub, G. W. Peterson, C. T. Buru, T. Islamoglu, O. K. Farha, *CrystEngComm* **2019**, *21*, 2409-2415.

[26] C. Avci-Camur, J. Perez-Carvajal, I. Imaz, D. Maspoch, *ACS Sustainable Chem. Eng*. **2018**, *6*, 14554-14560.

[27] S. Dai, F. Nouar, S. Zhang, A. Tissot, C. Serre*, Angew. Chem. Int. Ed*. **2021**, *60*, 4282-4288

[28] J. Hafizovic Cavka, S. Jakobsen, U. Olsbye, N. Guillou, C. Lamberti, S. Bordiga, K. P. Lillerud, *J. Am. Chem. Soc.* **2008**, *130*, 13850-13851.

[29] L. Valenzano, B. Civalleri, S. Chavan, S. Bordiga, M. H. Nilsen, S. Jakobsen, K. P. Lillerud, C. Lamberti, *Chem. Mater.* **2011**, *23*, 1700-1718.

[30] O. Egyed, *Vib. Spectrosc.* **1990,** *1*, 225-221

[31] S. Waitschat D. Fröhlich,H. Reinsch, H. Terraschke, K. A. Lomachenko, C. Lamberti, H. Kummer, T. Helling, M. Baumgartner, S. Henninger, N. Stock, *Dalton Trans*. **2018**, *47*, 1062-1070.

[32] Z. H. Rada, H.R. Abid, J. Shang, H. Sun, Y. He, P. Webley, S. Liu, S. Wang, *Ind. Eng. Chem. Res*. **2016**, *55*, 7924-7932.

[33] Z. Chen, X. Wang, T. Islamoglu, O. K. Farha, *Inorganics* **2019**, *7*, 56.

[34] M. J. Katz, Z. J. Brown, Y. J. Colón, P. W. Siu, K. A. Scheidt, R. Q. Snurr, J. T. Hupp, O. K. Farha, *Chem Commun*. **2013**, *49*, 9449–9451.

[35] H. Jasuja, G. W. Peterson, J. B. Decoste, M. A. Browe, K. S. Walton, *Chem. Eng. Sci.* **2015**, *124*, 118-124.

[36] X. Zhang, B. Shen, S. Zhu, H. Xu, L. Tian, *J. Hazard. Mater.* **2016**, *320*, 556-563.

[37] S. Biswas, J. Zhang, Z. Li, Y-Y. Liu, M. Grzywa, L. Sun, D. Volkmer, P. Van Der Voort, *Dalton Trans*. **2013**, *42*, 4730-4737.